

Preliminary Study on Enhancing Detection of Concrete Bridge Surface Spalling by Infrared Thermography

Ching-Wei Chen ¹, Hui-Ping Tserng ¹, En-Wei Chiang ¹

¹Department of Civil Engineering, National Taiwan University, Taipei, Taiwan.
D09521018@ntu.edu.tw, hptserng@ntu.edu.tw, r10521701@ntu.edu.tw

Abstract

Regular inspections, effective management, and timely maintenance are critical issues to ensure bridge safety and quality. Currently, visual inspection remains the predominant method employed worldwide for bridge inspection. However, visual inspection heavily relies on the training, experience, and subjective judgment of inspectors, leading to inconsistent assessments. When applying deep learning techniques to assist in identifying bridge crack formations, challenges persist. Some images may not clearly display the crack's location. Infrared thermography, with its non-contact, non-destructive properties, effectively detects surface delamination in concrete bridges. However, most research employs higher-spec infrared thermography, which comes with higher instrument costs and less economic viability. Hence, this study aims to investigate the feasibility of using lower-spec infrared thermography to detect surface delamination in concrete bridges as well as analyze the potential of using lower-spec infrared thermography results to assist AI image recognition of bridge surface defects.

Keywords –

Infrared Thermography; Bridge Inspection; Concrete Defects; Passive Infrared Thermography technology; AI Image Recognition

1 Introduction

Regular inspections, effective management, and timely maintenance are critical issues to ensure bridge safety and quality. Currently, visual inspection remains the predominant method employed worldwide for bridge inspection. However, visual inspection heavily relies on the training, experience, and subjective judgment of inspectors, leading to inconsistent assessments.

As for the literature review related to this research objectives, Yahui Liu et al. (2019)[1] propose a deep hierarchical convolutional neural network (CNN) to detect the concrete crack without using thermal imaging cameras. Chia-Chi Cheng et al. (2008) [2] use infrared

thermography associated with elastic waves to detect concrete structure defects in the lab. Using this elastic waves in the lab maybe not suitable for this research utilizing to the bridge. This study utilizes the test method modified from ASTM [3] to detect cracks in concrete using infrared thermography. Rocha and Povoas (2017)[4] just review the state of the art using infrared thermography to inspect the concrete bridges. However, the infrared instruments used in these literature [3,4] are too heavy and large to be employed on unmanned aerial vehicles (UAV). For next further research objectives, it will be utilized a lighter and smaller infrared instrument to employ the defect detection with UAV. Nevertheless, there is still a significant challenge to overcome AI image recognition. Previous literature has highlighted the effectiveness of thermal imaging cameras in detecting concrete bridge surface spalling. Currently, this study first aims to investigate the feasibility of employing low-standard infrared thermal imaging cameras (lighter and smaller) to detect concrete bridge surface spalling and support AI image recognition technology in bridge inspections. In the further research, this lighter and smaller infrared instrument can be easily to be employed to the defect detection with UAV.

Based on laboratory research and on-site inspections of bridges, the FLIR E5 infrared thermal imaging camera has demonstrated the recommended measurement distance of 1 to 2 meters. While it may not be suitable for measuring shallow-depth and small-area defects, it excels in effectively detecting various shapes of spalling and supporting AI image recognition. Consequently, employing low-standard infrared thermal imaging cameras for the detection of concrete bridge surface spalling and integration with AI image recognition technology in bridge inspections appears to be a feasible approach.

2 Methodology

2.1 Research Procedure

This research first comprehends the background of bridge inspection and infrared inspection in Taiwan. It

describes the research motivations, objectives, scope, and limitations, followed by a literature review that gathers relevant domestic and international studies along with pertinent theories. After the literature review, laboratory experiments and on-site bridge inspections will be conducted. In the laboratory experiments, dimensions of test specimens and defect sizes will be determined based on multiple domestic and international studies. Test specimens will be created according to the actual composition of Taiwanese concrete bridges (designed strength of 350 kgf/cm²). The entire process of specimen creation, including template assembly, material preparation, mixing, defect model creation, grouting, and final curing, will be executed independently. During the first phase of experiments, equipment suitability (FLIR E5, shown in Figure 1 and 2)) for measurement dimensions and distances will be determined based on the analysis results. The second phase will primarily explore whether defects of different shapes can be detected similarly. The third phase will involve redesigning and creating new specimens, conducting thermal imaging analysis to assist Deepcrack AI image recognition, and drawing final conclusions. In the bridge inspections, identical measurement and analysis methods will be employed to derive conclusive results.

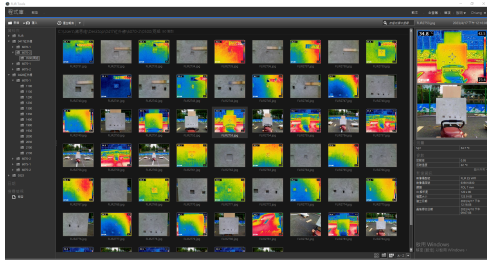


Figure 1. FLIR tools/tools+ software screenshot



Figure 2. FLIR tools/tools+ Software editing model

2.2 Bridge Crack Inspection Experiments

2.2.1 First-Phase of Experiment

The concrete specimens in this study will be fabricated to match the actual design strength of Taiwanese concrete bridges, which is 350 kgf/cm². The dimensions of the concrete specimens will be 60×70×10 cm³, with the defective portions made using perlite

boards whose sizes vary according to the experimental phases. The concrete mix will have a water-cement ratio of 0.55, requiring 18.9 kg of cement, 11.1119 kg of water, 29.8918 kg of mainland sand, and 41.2113 kg of coarse aggregates.

Passive infrared thermography will be utilized in this phase of experiments. The prepared specimens will be laid flat in an area devoid of shadows and exposed to direct sunlight. When capturing images, the concrete specimens will be positioned upright, and the FLIR E5 infrared camera will conduct two sets of captures every half hour. Each set will encompass five measurement distances (1m, 2m, 3m, 4m, 5m). Image capture sessions are scheduled from 11:00 a.m. to 2:00 p.m. and from 7:00 p.m. to 9:30 p.m. A distance meter, UNI-T LM80, will ensure the infrared camera is perpendicular to the specimen, and an infrared thermometer, TECPEL-DIT300B, will measure the surface temperature of the specimen.

2.2.2 Second and Third-Phase Experiments

In this phase of the experiment, passive infrared thermography will be employed, and the fabricated specimens will be laid flat in an area without shadows and exposed directly to sunlight. During the capture process, the operator will stand on an A-frame ladder and utilize the FLIR E5 infrared camera to capture images in sets every half hour. Each set will involve two measurement distances (1m, 2m), and the image capture sessions will occur from 3:00 p.m. to 5:00 p.m. A distance meter, UNI-T LM80, will ensure the infrared camera is perpendicular to the specimen, and an infrared thermometer, TECPEL-DIT300B, will measure the surface temperature of the specimen.

2.3 Data Collections

The temperature data acquisition through thermal imaging will be performed using FLIR tools to obtain the average temperature of the defect (T_i) and the average temperature around the defect (T_S). The steps are as follows:

- (1) Import the desired image into FLIR tools (using defect number 1 for demonstration purposes). Double-click to open the image and enter the operating interface. Switch the image mode to digital thermal camera (visible light image).
- (2) In the visible light image within the digital thermal camera mode, use the temperature measurement function to select the area of the defect for measurement. This action will yield the average temperature of the defect. For demonstration purposes using defect number 1 from the first set of specimens (refer to Figure 3), the average temperature (T_1) of defect number 1 (Bx1) is measured to be 42.5°C.



Figure 3. Example of selecting defect temperature value in the visible light image

1. The selected area on the defect measures 40×40 (Figure 4) in pixels, representing 1600 temperature values within the selected area. When comparing the 40×40 (pixels) area to the actual defect size of 10×10 (cm²), there exists a 4:1 ratio. Therefore, in this study, the perimeter of the defect is extrapolated to 3 centimetres from the defect distribution (Figure 5), meaning the real size is 16×16 (cm²). FLIR tools utilize a size of 64×64 (pixels). In this example, after the selection process, the overall average temperature (T_A) within the 64×64 (pixels) area is measured at 41.9°C (marked as Bx2 in Figure 5).

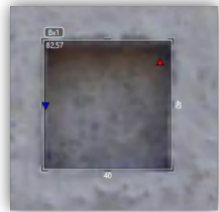


Figure 4. Diagram illustrating defect selection in digital thermal camera image mode

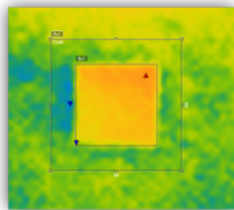


Figure 5. Diagram illustrating selection in infrared imaging mode

2. However, the overall average temperature value (T_A) within the selected 64×64 (pixels) area in Step 3 includes the temperature of the defect itself. To obtain the defect's surrounding average temperature (T_S) required for this study, this temperature should be deducted. Therefore, by employing the following formula:

$$T_s = \frac{T_A \times A_t - \sum_{i=1}^n T_i \times A_i}{A_t - \sum_{i=1}^n A_i} \quad (1)$$

T_s : Defect surrounding average temperature

T_A : Overall average temperature

T_i : Defect average temperature

A_t : Total area

A_i : Defect area

i : Defect number

The obtained defect surrounding average temperature (T_S) is 41.52°C. According to the defect assessment method adopted by ASTM-D4788 in this study, to identify concrete defects in thermal imaging, the temperature of the defect must differ by at least 0.5°C from the adjacent area. In the demonstrated example, the temperature difference (Δ_T) is calculated by subtracting the average temperature of defect number 1 (T_1) from the defect surrounding average temperature (T_S), resulting in 0.98°C. As this value is greater than or equal to 0.5°C, it indicates that defect number 1 in this example has been successfully detected as a defect.

$$\Delta_T = T_1 - T_s = 0.98 \geq 0.5 \text{ (}^\circ\text{C)} \quad (1)$$

3 Research Results

In both the first and second phases of the experiment, the research results will be presented using line graphs (as in Figure 6) and pie charts (as in Figure 7). The third stage will involve the use of line graphs and bar charts for discussion purposes. For on-site bridge inspections, discussions will be presented in tabular form. The following is a summary of the three stages of the experiment.

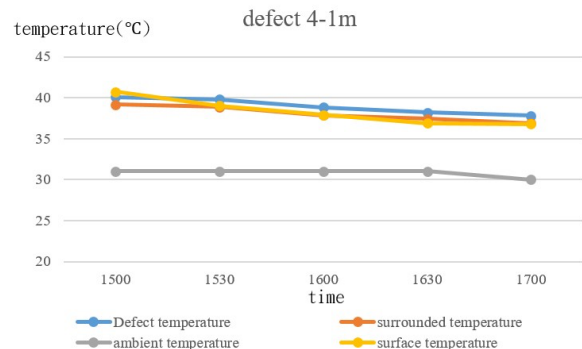


Figure 6. The line graph for defect number 4 of the third set of specimens, taken at a distance of 1 meter on the thermal image between 3:00 p.m. and 5:00 p.m.

| The total number of measurements for a distance of 1m | 30 | | | | | | | |
|---|-----|-----|-----|-----|-----|-----|-------|--|
| Defect number | 1 | 2 | 3 | 4 | 5 | 6 | total | |
| Detectable number | 5 | 4 | 4 | 5 | 5 | 5 | 28 | |
| ratio | 17% | 13% | 13% | 17% | 17% | 17% | 93% | |

Detectable proportion of different defect shapes when measuring distance 1m

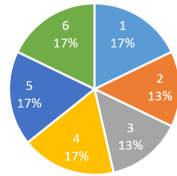


Figure 7. Pie chart depicting the detection rates of different defect shapes at a distance of 1 meter.

3.1 Result of first-phase experiment

1. The relative area of the defect's depth significantly affects detection outcomes, with sizes smaller than 1 centimeter in depth proving less detectable by the FLIR E5 infrared thermal imager utilized in this study.
2. Defects with a depth of 3.5 centimetres but an area smaller than 1 square centimetre are challenging to detect with the equipment employed in this research.
3. The recommended measurement distance for the equipment used in this study is between 1 to 2 meters, allowing for the detection of a broader range of sizes. The average measurement error is also smaller, consistently below 5%.
4. The detection rate in this stage of experiments was notably low, attributed to insufficient sunlight exposure. Adjustments in measurement timings during the second stage aim to enhance the detection rate.

3.2 Result of Second-phase experiment

1. For the thermal imager FLIR E5 utilized in this study, the detectability at a measurement distance of 1 meter is 93%, and at 2 meters, it is 90%. This indicates a substantial increase in detection rates during the 3:00 p.m. to 5:00 p.m. period compared to the first stage's imaging sessions from 11:00 a.m. to 2:00 p.m.
2. The FLIR E5 thermal imager employed in this research can detect not only rectangular defects but also various other shapes, aligning with practical applications in bridge inspection.

3.3 Result of Third-phase experiment

1. Infrared thermal imaging results indicated a recognition rate of 38% for the fourth set of specimens (pure cracks) and 88% for the fifth set

(cracks with localized delamination). This suggests that the presence of localized delamination around cracks contributes to enhancing passive infrared thermal imaging detection.

2. In Deepcrack AI image recognition, the detection rate for the fourth set of specimens (cracks) stood at 100%, surpassing the detection rate of 88% for the fifth set (cracks with localized delamination). This indicates that localized delamination might potentially lower the detection rate in Deepcrack AI image recognition.
3. During false defect recognition in Deepcrack AI image recognition, the misjudgement rates for the fourth set of specimens (pure cracks) and the fifth set (cracks with localized delamination) were 63% and 50%, respectively. However, in infrared thermal imaging, the misjudgement rates for both were 0%.

Based on the above, it's evident that infrared thermal imaging effectively assists AI image recognition in defect detection. Defects with very shallow depths or small areas may not be detectable by the FLIR E5 infrared thermal imager used in this study. However, given that practical applications often prioritize identifying larger or deeper defects that pose higher risks, the method used in this study is suitable for bridge inspection practices.

4 Conclusion

1. Based on the experimental results, this study recommends using the FLIR E5 infrared thermal imager for imaging at an optimal measurement distance of 1 to 2 meters. This range effectively detects larger, deeper, and variously shaped defects posing higher risks.
2. Laboratory research and on-site bridge inspections indicate that the FLIR E5 infrared thermal imager is less suitable for measuring defects with shallower depths or smaller areas. However, defects with shallower depths or smaller areas do not significantly impact bridge safety.
3. The detection rate significantly improves during imaging sessions between 3:00 p.m. and 5:00 p.m. compared to those from 11:00 a.m. to 2:00 p.m., suggesting that using passive infrared thermal imaging for defect detection is advisable when the subject has adequate exposure to heat.
4. The study observed that elongated and small-area defects resembling cracks are less detectable by the FLIR E5 infrared thermal imager used in this research. However, the presence of localized delamination around cracks enhances the effectiveness of passive infrared thermal imaging.
5. In the third stage of experiments, it was found that

the presence of localized delamination around cracks improves the detection rate of passive infrared thermal imaging but lowers the detection rate of AI image recognition. Additionally, AI image recognition exhibits a significantly higher false defect identification rate compared to infrared thermal imaging.

The contribution of this work is to confirm that smaller and lighter infrared devices can enhance the accuracy of detecting concrete cracks. These smaller and lighter devices can be easily installed on unmanned aerial vehicles in the future research to conduct real-time bridge inspection work.

References

- [1] Yahui Liu, Jian Yao, Xiaohu Lu, Renping Xie, Li Li (2019) .Deepcrack : A deep hierarchical feature learning architecture for crack segmentation.
- [2] Chia-Chi Cheng, Tao-Ming Cheng, Chih Hung Chiang, (2008). Defect detection of concrete structures using both infrared thermography and elastic waves.
- [3] D4788 - ASTM (1997): Standard Test Method for Detecting Delaminations in Bridge Decks Using Infrared Thermography.
- [4] J. H. A. Rocha, Y. V. Povoas (2017). Infrared thermography as a non-destructive test. for the inspection of reinforced concrete bridges : A review of the state of the art.